npj | Flexible Electronics

www.nature.com/npjflexelectron

REVIEW ARTICLE OPEN

Flexible quantum dot light-emitting diodes for next-generation displays

Moon Kee Choi[1,2], Jiwoong Yang[1,2], Taeghwan Hyeon[1,2] and Dae-Hyeong Kim[1,2]

In the future electronics, all device components will be connected wirelessly to displays that serve as information input and/or output ports. There is a growing demand of flexible and wearable displays, therefore, for information input/output of the next-generation consumer electronics. Among many kinds of light-emitting devices for these next-generation displays, quantum dot light-emitting diodes (QLEDs) exhibit unique advantages, such as wide color gamut, high color purity, high brightness with low turn-on voltage, and ultrathin form factor. Here, we review the recent progress on flexible QLEDs for the next-generation displays. First, the recent technological advances in device structure engineering, quantum-dot synthesis, and high-resolution full-color patterning are summarized. Then, the various device applications based on cutting-edge quantum dot technologies are described, including flexible white QLEDs, wearable QLEDs, and flexible transparent QLEDs. Finally, we showcase the integration of flexible QLEDs with wearable sensors, micro-controllers, and wireless communication units for the next-generation wearable electronics.

npj Flexible Electronics (2018)2:10 ; doi:10.1038/s41528-018-0023-3

INTRODUCTION

Flexible displays have received significant attention owing to their potential applications to mobile and wearable electronics[1,2] such as smartphones, automotive displays, and wearable smart devices. Displays with flexible form factors have thin, lightweight, and nonbreakable characteristics, which enable the fabrication of displays on curvilinear surfaces and allow their shapes to be transformed.[3,4] In 2008, Nokia announced Morph, an innovative mobile display concept with flexible, bendable, and interactive features. This was followed by the development of early prototypes of flexible e-paper. In 2013, Samsung Electronics demonstrated the first curved television (TV) based on organic light-emitting diodes (LEDs) that feature a wide field of view, high color purity, and outstanding contrast. Two years later, the same company reported a smartphone with the curved edge display (Galaxy S6 edge) that used a curved organic LED display panel with touch sensors to improve the user interface and device design.

Although non-flat displays are being marketed, the currently available commercialized displays are mostly bent displays whose shape cannot be changed. The next-generation display, by contrast, will be transformable into various forms.[5–7] Figure 1 shows representative examples of future interactive displays with flexible form factors. Smart glasses and/or smart lens (Fig. 1a) will enable augmented reality, displaying information additively over the natural scene behind the glasses or lens. It will be possible to display vital signs (*e.g.*, blood pressure, pulse, respiration rate, and body temperature) or other health information measured by a wearable sensor in real-time through smart watches (Fig. 1b). LEDs fabricated in the form of yarns can be woven into fabric and cloth for wearable displays (Fig. 1c). Ultrathin displays will be attached to the human skin in the form of electronic tattoos (Fig. 1d). Bendable displays can be utilized as foldable tablets whose screen sizes are tunable (Fig. 1e). Moreover, transparent flexible displays can be used for smart windows or digital signage, which can display digital information overlapped on the background view (Fig. 1f).

A major technological goal in the research field of such next-generation displays is to develop LEDs with mechanical deformability as well as excellent device performances.[8] Inorganic LEDs (iLEDs) have shown high brightness (10^6–10^8 cd m^{-2}) and low turn-on voltages (<2 V) and have been used to develop flexible LED arrays. However, thick and brittle active layers (~micrometers) limit their flexibility, and the point-array design cannot realize a high-resolution display (Table 1, i).[9,10] Organic LEDs (OLEDs; Table 1, ii) and polymer LEDs (PLEDs; Table 1, iii) have become a hot research topic because the self-luminous active layer simplifies the device structure, which can drastically reduce the entire thickness of the display.[11,12] Recently, LG Electronics introduced a 66-inch ultra-large TV at SID 2017, which reduced the total panel thickness down to 1 mm. However, the flexibility of the current OLED display is still limited by thick encapsulation layers (*e.g.*, it allows bending rather than folding or stretching). It is essential to develop thin encapsulation layer which endures continuous bending stress and effectively prevents oxidation of organic active layer, organic charge transport layer and thin metal electrode. The long-term electroluminescence (EL) stability and achievement of high color purity also remain practical challenges of OLEDs.

Recently, quantum dot LEDs (QLEDs) have received great attention because of their outstanding color purity (full-width-at-half-maximum (FWHM) ~30 nm), high brightness (up to ~200,000 cd m^{-2}), low operating voltage ($V_{\text{turn-on}}$ < 2 V), and easy processability (Table 1, iv).[13–15] The high thermal and air stabilities

[1]Center for Nanoparticle Research, Institute for Basic Science (IBS), Seoul 08826, Republic of Korea and [2]School of Chemical and Biological Engineering, Institute of Chemical Processes, Seoul National University, Seoul 08826, Republic of Korea
Correspondence: Taeghwan Hyeon (thyeon@snu.ac.kr) or Dae-Hyeong Kim (dkim98@snu.ac.kr)
Moon Kee Choi and Jiwoong Yang contributed equally to this work.

Received: 14 October 2017 Revised: 20 January 2018 Accepted: 26 January 2018
Published online: 05 April 2018

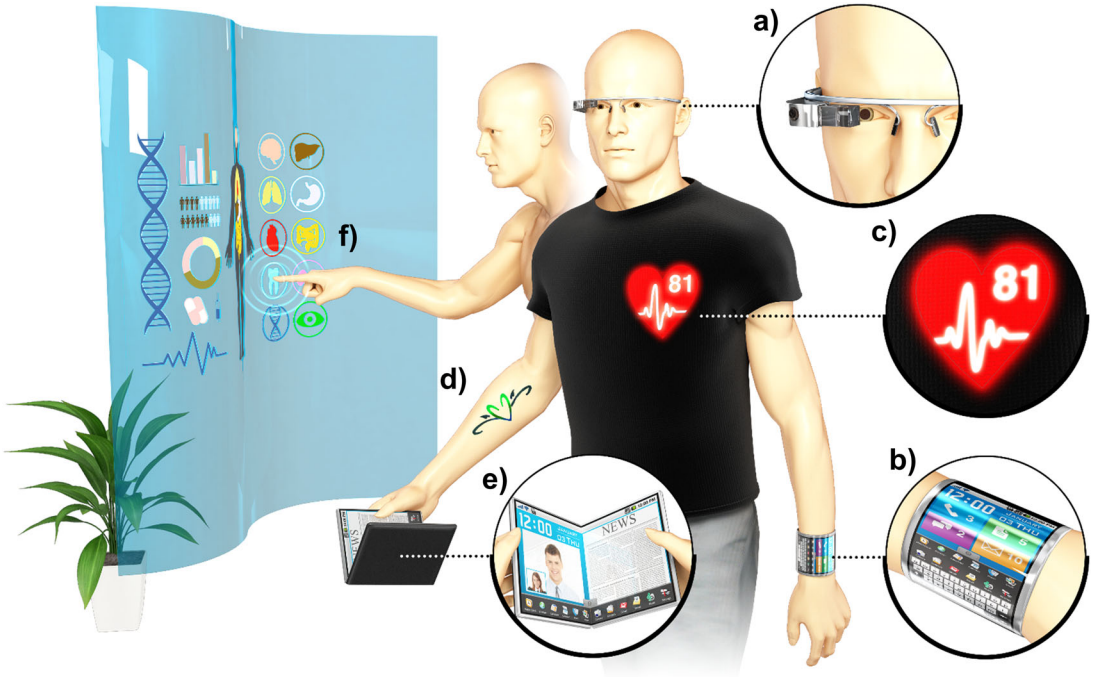

Fig. 1 Future of flexible and wearable displays. **a** Smart glasses or smart lens. **b** Smart watch with wearable biosensors. **c** fabric display. **d** Ultrathin electronic tattoo. **e** Bendable and foldable display. **f** transparent smart windows

Table 1. Representative characteristics of different types of light-emitting didoes

Type	(i) iLED	(ii) OLED	(iii) PLED	(iv) QLED
Max. brightness	10^6–10^8	10^2–10^4	10^2–10^4	10^3–10^5
Fabrication	MBE and MOVPE	Spin coating and vacuum evaporation	Spin coating	Spin coating
Color purity	~20–100 nm	~100 nm	~100 nm	~30 nm
Operating voltage	–	2–10 V	2–10 V	2–10 V
Stability of active materials	High	Low	Low	High
Active layer thickness	>Several micrometers	<100 nm	<100 nm	<100 nm

of the inorganic quantum dots (QDs) enables the enhanced lifetime and durability of the display. In addition, the recent advances in patterning techniques have made it possible to achieve ultrahigh-resolution full-color (red, green, and blue; RGB) QLED array, which could not be implemented with the conventional display processing technologies (*e.g.*, shadow masking in OLEDs). More detailed characteristics of the aforementioned LEDs with different types of light emitting layers (*e.g.*, inorganic, organic, polymer, and QD) are summarized in Table 1.

Here, we thereby focus on QLEDs among the various types of light-emitting devices toward the next generation flexible displays. First, we review the synthesis strategies for highly efficient and stable QD emitters, the device structure engineering and operation principles of each structure, and the patterning technologies for full-color QD displays. Then we describe the recent technological advances in QLEDs such as flexible white QLEDs and transparent version of flexible QLEDs. Finally, this review introduces integrated systems using flexible QLEDs as informative displays for wearable electronics and concludes with a brief outlook.

MATERIAL DESIGN FOR EFFICIENT QLEDS

It is worthwhile to introduce the recent development of QLEDs, because it is highly related to the advance of flexible/wearable QLEDs. In this section, we discuss materials chemistry of QDs, which enables effective operation of QLEDs. QDs have many advantages in display applications, originating from the quantum-confinement effect.[16–24] For example, emission wavelengths of CdSe QDs can be tuned by changing their size to emit the entire visible light (Fig. 2a).[25] In addition, QDs based on various semiconductor materials provide broad spectral window and chemical versatility (Fig. 2b, c).[26–34] High color purity is also an important characteristic for display applications. CdSe QDs show very sharp emission spectra (FWHM of ~30 nm) and wide color gamuts compared to the conventional standard emission spectra of the commercialized high-definition television (Fig. 2d).[35–37]

Type I core/shell QDs are commonly employed in QLEDs (Fig. 2e), because overcoating the core QDs with wide band gap shell materials passivates surface defects and confines excitons to the cores.[38–43] This leads to significant improvements in stability and the photoluminescence quantum yield (PLQY) that is directly proportional to the external quantum efficiency ($EQE = n \times \chi \times \eta_{PL} \times \eta_{oc}$). For example, CdSe/ZnS QDs exhibit high PLQY of 70–95%, which is an order of magnitude higher than that of bare QDs. However, the increase in PLQY does not guarantee the enhanced EL performance. Auger recombination of charged QDs and/or interparticle energy transfer between different QDs reduce the EL efficiency. These processes are dramatically affected by the structure of the core/shell interfaces, and consequently the

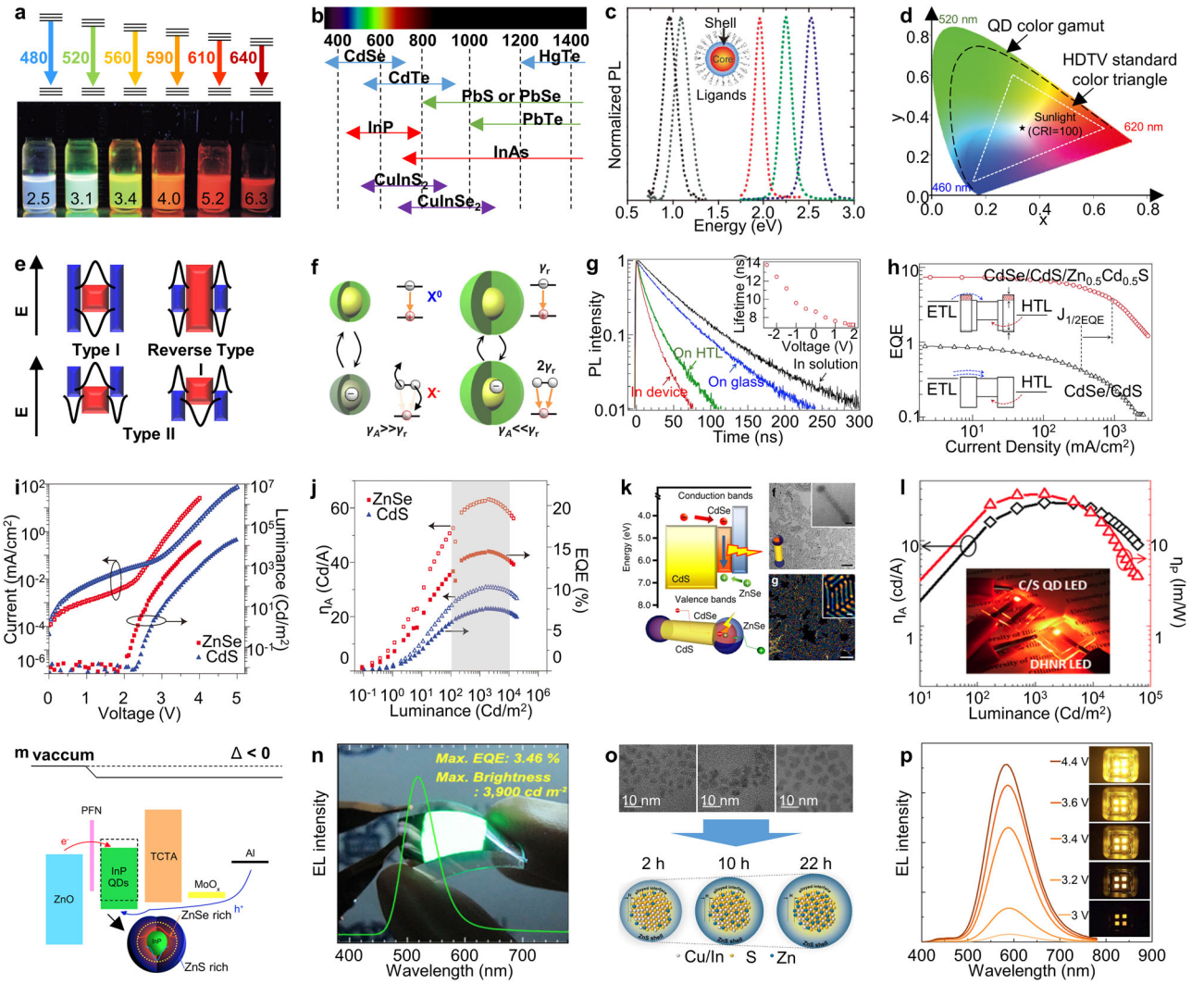

Fig. 2 Material designs for efficient QLEDs. **a** Photograph of solutions containing CdSe QDs of various sizes, showing emission color covering the entire visible light range. **b** Spectral range of QDs with various semiconductor materials. **c** PL spectra of CdSe/ZnS and PbS/CdS core/shell QDs. **d** CIE chromaticity diagram showing the color gamut of CdSe QDs in comparison with that of conventional high-definition television standards. **e** Scheme showing the band structure of core/shell heterojunctions. **f** Scheme comparing the carrier dynamics of core/shell QDs with thick and thin shells. **g** Time-resolved PL spectra of QDs under various conditions. The inset shows the change in the carrier lifetime as a function of applied voltage. **h** Comparison of EQEs of QLEDs with CdSe/CdS core/shell QDs and CdSe/CdS/$Zn_{0.5}Cd_{0.5}S$ core/shell/shell QDs. **i**, **j**, Current density–luminance–voltage characteristics (**i**), current efficiency and EQE (**j**) of QLEDs using CdSe/ZnS QDs with CdS-rich (blue) and ZnSe-rich (red) intermediate shells. **k** Energy band diagram, schematic, and TEM images of double heterojunction nanorods. **l** Current and power efficiencies of QLEDs based on double heterojunction nanorods as a function of luminance. The inset show a photograph comparing double heterojunction nanorod QLEDs and conventional core/shell QLEDs. **m** Energy diagram of InP@ZnSeS QLEDs. **n** EL spectrum and photograph of flexible InP@ZnSeS QLEDs on a polyethersulfone substrate. **o** TEM images and corresponding schematic images of Cu–In–S/ZnS QDs with controlled shell thickness. **p** EL spectra and corresponding images of Cu–In–S/ZnS QLEDs as a function of applied voltage. Figure reproduced with permission from: **a** ref. [25] © 2010 Wiley; **c** ref. [26] © 2010 Nano Reviews; **f** ref. [46] © 2012 NPG; **g**, **h** ref. [47] © 2013 NPG; **i**, **j** ref. [52] © 2015 NPG; **k** ref. [53] © 2014 NPG; **l** ref. [54] © 2015 ACS; **m**, **n** ref.[69] © 2013 ACS; **o**, **p** ref. [73] © 2016 ACS

structure modification of the core/shell QDs has become an important issue.

The simplest way of controlling the core/shell structure is to modify the shell thickness, which affects significantly the carrier dynamics of QDs as well as their stability. QDs with thick shells are less blinking (or nonblinking) because of either suppression of charge fluctuations or enhancement of the PLQY of charged QDs (Fig. 2f).[44–46] The enhanced PL dynamics in thick-shell QDs can improve device performance significantly. As shown in Fig. 2g, QDs in devices are easily charged by excessive charge carriers (electrons in this case). Thicker shell helps to suppress charging of QDs during light emission of QLEDs, which results in the improved EL efficiency (Fig. 2h).[47–51] The composition of the core/shell interface is also important for the carrier injection and recombination. Recently, two types of CdSe/ZnS core/shell QDs with similar PLQY and bandgaps were compared based on the composition of their core/shell interface: QDs with ZnSe-rich intermediate shells and QDs with CdS-rich intermediate shells (Fig. 2i, j).[52] ZnSe-rich QDs demonstrated superior EL properties, which were attributed to the low carrier injection barrier of ZnSe-rich QDs. Currently, the composition of core/shell interface has been controlled roughly, and its impact on the EL mechanism has yet to be fully understood. A major limiting factor in these efforts is the lack of characterization methods that can determine precisely the three-dimensional composition distribution of core/shell QDs.

Structure engineering of QDs improves not only carrier dynamics but also other factors such as light outcoupling. For example, QLEDs based on double-heterojunction nanorods show unexpected enhancement of EL performance (maximum brightness = 76,000 cd m^{-2}, peak EQE = 12%) (Fig. 2k, l).[53–55] In this structure, two CdSe emitters are directly connected to CdS nanorods and the remaining surface of CdSe is passivated by ZnSe. Remarkably, the obtained peak EQE (12%) was higher than the expected upper limit (8%) considering their PLQY (40%). It was suggested that the shape anisotropy and directional band offsets of the double-heterojunction nanorods could improve light outcoupling.

Along with the recent progress, there have been growing concerns regarding the use of QDs containing the Cd element, which is very harmful for the human body and environment.[56–62] This issue become more significant in flexible/wearable displays, where the device is in direct contact with the human body. For instance, the European Union's Restriction of Hazardous Substances Directive regulates the use of Cd-based compounds in consumer electronics. Although several approaches such as encapsulation, or minimization of Cd concentration by composition control have been reported, it is clear that the development of efficient heavy-metal-free QLEDs is ultimately required for the commercial success of flexible/wearable QLEDs.

III-V InP QDs are promising alternatives to Cd-chalcogenide QDs because their bandgaps cover the entire visible range (bulk bandgap = 1.34 eV) with outstanding PLQYs.[63–66] Although there have been several reports on InP QLEDs, a gap remains in terms of the performance of InP QLEDs and that of Cd-chalcogenide QLEDs,[67,68] which can be attributed to the lack of fundamental understanding of the EL process of InP QDs. Recent progress on QLEDs based on green InP core–shell QDs is encouraging (Fig. 2m, n); record EQE[69] = 3.4%, record brightness[70] = 10,490 cd m^{-2}. Another important approach is the utilization of I–III–VI semiconductor QDs (Fig. 2o, p).[71–74] A critical drawback of I–III–VI QDs is their broad emission spectra (FWHM: ~100 nm), which removes the major advantage of QDs (i.e., high color purity due to narrow spectra) in display applications.[75]

DEVICE STRUCTURE AND OPERATION PRINCIPLES OF QLEDS

Basically, the device structure of flexible/wearable QLEDs are largely adopted from the general QLEDs with several modifications to achieve high deformability. The general structure of QLEDs consists of an anode, electron transport layers (ETLs), QD layers, hole transport layers (HTLs), and a cathode (Fig. 3a). The working mechanism of QLEDs is as follows: (i) electrons and holes are injected from electrodes into charge transport layers (CTLs); (ii) the carriers are injected into QDs from CTLs; and (iii) radiative recombination of the injected carriers takes place in QDs (Fig. 3b). The performance and stability of QLEDs are largely dependent on the choice of CTL materials. Good CTLs should have the high carrier mobility and balance the electron/hole injections well.

According to the type of CTLs employed, the structure of QLEDs can be categorized into four different types (Fig. 3c): (i) organic/QD bilayer; (ii) all-organic CTLs; (iii) all inorganic CTLs; and (iv) organic–inorganic CTLs. Their device performances in terms of the peak EQE and maximum brightness are summarized in Fig. 3d, e. Owing to its simplicity, the type (i) structure (organic/QD bilayer) was commonly used in the earliest QLEDs.[76–78] However, the electron injection was poorly controlled, and the leakage current was significant (maximum brightness ~100 cd m^{-2}, EQE <0.01%) because of the absence of ETLs and poor physical separation of QDs and CTLs. To solve these issues, the type (ii) device (QD layers sandwiched between organic HTLs and ETLs) was proposed.[79–84] The peak EQE of the initial type (ii) device was ~0.5% and has been improved to 6% (Fig. 3d, e).

Inorganic materials are among the most important choices for CTLs (type (iii) QLEDs; all-inorganic CTLs) owing to their high electrical conductivity and good stability against environmental factors such as oxygen and moisture. In the initial study, QD layers were sandwiched between *p*-type and *n*-type GaN (EQE <0.01%).[85] In the following works, QLEDs with all-inorganic CTLs composed of metal oxides (*e.g.*, ZnO, SnO_2, ZnS, NiO, and WO_3) were demonstrated.[86–88] These devices exhibited superior stability under long-term usage and high-current-density conditions, which would be potentially beneficial for future flexible display applications. However, the overall device performance was poor as a result of the degradation of QDs during the harsh deposition process of inorganic layers.

The type (iv) structure (usually organic HTLs and inorganic ETLs) was developed to take advantage of both inorganic and organic CTLs. Although their performance did not improve significantly (EQE of ~0.2%) in the initial work 89, an important breakthrough was made by introducing ZnO nanoparticles as ETLs.[90–96] ZnO exhibits excellent electron mobility even in the form of nanoparticles, and no significant damage occurs to the underlying QD layers during the introduction of these nanoparticles in the device because they are solution processable. Currently, because of their excellent EL performance (see Fig. 3d, e for comparison), type (iv) devices using ZnO nanoparticles as ETLs have become a standard in the QLED research[48,52,97,98] including flexible devices. Another important benefit of these devices is the ultrathin form factor (hundreds of nanometers) of overall layers, which makes them suitable for flexible displays. For example, one of the recent studies demonstrated the highly deformable wearable QLEDs whose total thickness is less than 3 μm including device parts and double-layered encapsulation layers.[99] More information on ultrathin encapsulation layers for flexible QLEDs is available in the following section on wearable quantum dot displays.

PATTERNING TECHNOLOGY OF QDS FOR FULL-COLOR DISPLAYS

Significant efforts have been made to achieve high-resolution full-color QD-based displays, including flexible ones. Especially, wearable and/or portable electronics integrated with flexible display need high resolution and full color form to present vivid visual information within limited space. As the display technology has evolved, the resolution of TVs has reached the ultra-high definition (UHD; 3840 × 2160) level, and that of smartphone has become as high as ~800 pixels per inch (ppi). For instance, the pixel resolution of Xperia XZ premium (Sony) is 807 ppi. To show natural and clear images, the demand for the higher resolution displays is expected to increase further, as displays with the finer pixel resolution can express more vivid images. In case of the head-mount displays or virtual-reality displays, where flexible displays can be applied, implementation of even higher resolution displays is required to project three-dimensional synaptic images by magnifying the original two-dimensional images. There are two major approaches to patterning and integrating differently colored QDs with high resolutions onto the display panel—transfer printing[100] and inkjet printing.[101]

Since the as-synthesized colloidal QDs are dispersed in a solution phase, the spin-casting process was typically used in the early QLED studies, which led to monochromatic light-emitting devices. Later, a structured elastomeric stamp (usually a poly (dimethylsiloxane) (PDMS) stamp) was used to make pixelated QD patterns. In 2008, the Bawendi and Bulović group reported QLEDs patterned with lines and spaces, prepared by directly spin-casting the QD solution onto a structured stamp.[102] Later, the researchers at the Samsung Advanced Institute of Technology (SAIT) developed a kinetically controlled transfer-printing technology.[97] The spin-coated QD film was contacted with a structured stamp, quickly picked up from the self-assembled monolayer-treated

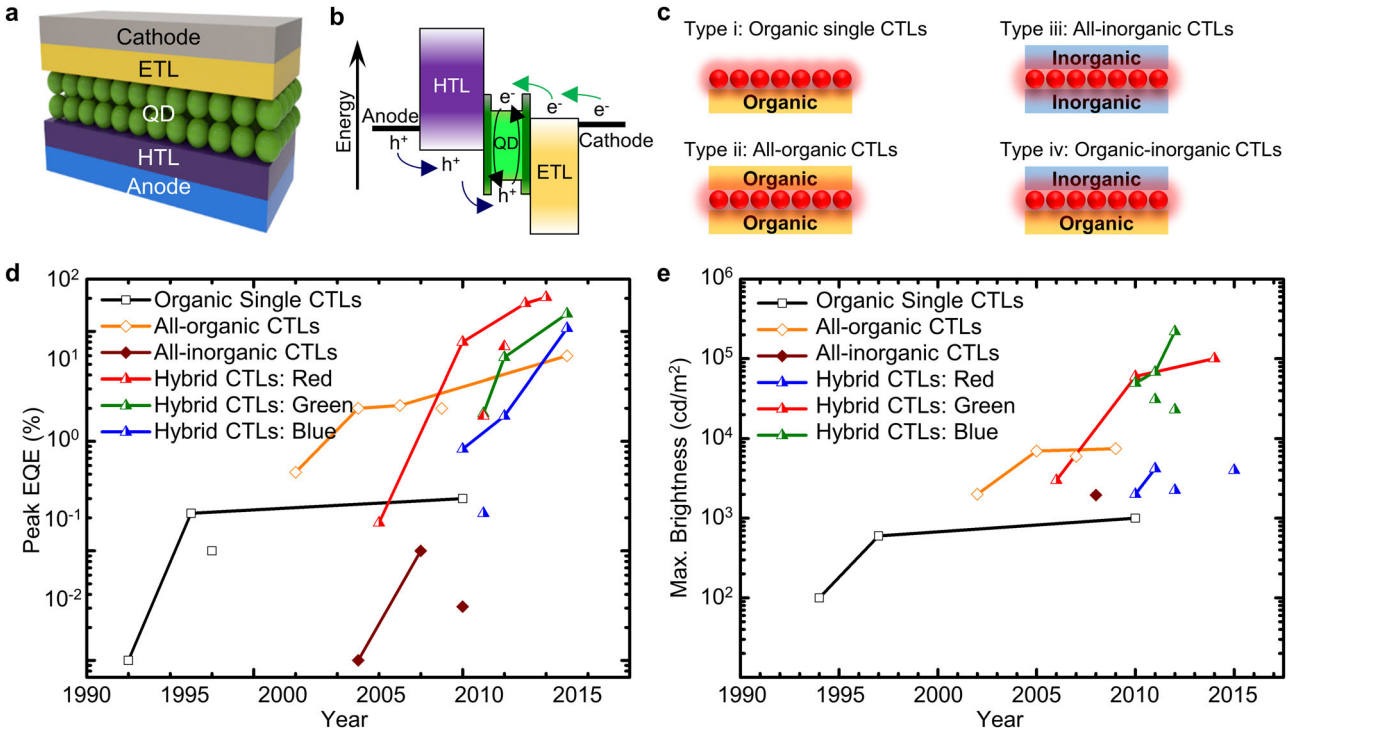

Fig. 3 Device structure and operation principles of QLEDs. **a** Representative device structure of quantum dot light-emitting diodes (QLEDs). **b** Energy diagram of a typical QLED showing charge injections from the anode and cathode. **c** Four representative device types of QLEDs according to the type of charge transport layer (CTL): (i) organic polymer CTL, (ii) all-organic CTL (*e.g.*, TPD and TPBi), (iii) all inorganic CTL (*e.g.*, *n*-type and *p*-type GaN), and (iv) organic (*e.g.*, TFB)–inorganic (*e.g.*, ZnO) CTL. **d**, **e** Progress in the performance of QLEDs in terms of peak external quantum efficiency (EQE) (**d**) and maximum brightness (**e**). The data are categorized according to the type of CTL (From type (i) to (iv) in **c**). Data for **d** are taken from references. (i) organic single CTLs: 76, 77, 78, 110, (ii) all-organic CTLs: 79, 80, 82, 83, 84, (iii) all-inorganic CTLs: 85, 86, 88, (iv) hybrid CTLs: 52, 89, 92, 93, 94, 95, 96. Data for panel **e** are taken from references: (i) organic single CTLs: 76, 77, and 110, (ii) all-organic CTLs: 79, 80, 82, and 83, (iii) all-inorganic CTLs: 86, (iv) hybrid CTLs: 48, 52, 89, 92, 93, 94, and 98

donor substrate, and released onto the desired substrate (Fig. 4a). As a result of the pressure applied by the stamp (Fig. 4b), the printed QD layer showed less vacancies and cracks after transfer printing than the QD patterns formed by other patterning methods. This well-packed QD layer led to low leakage current and improved charge transport, as shown in the current density—voltage (*J*–*V*) curve (Fig. 4c). Using this transfer printing method, a 4-inch full-color flexible display with 320×240 pixels was successfully demonstrated.

Although many patterning technologies were developed, extremely high resolution and printing yields could not be achieved. Therefore, to obtain pixels with higher definitions and yields, Choi *et al.* proposed an intaglio transfer-printing technique that could pattern a 2460 ppi red-green-blue (RGB) QD array.[99] Unlike the technique base on structured stamps, the QD patterns were defined when the stamp, fully inked with QDs, was contacted to and released from the intaglio trench made on the Si wafer (Fig. 4e). The difference in the interfacial energies ($E_{QD\text{-}trench} >> E_{QD\text{-}stamp}$) enabled a much higher transfer yield without cross-contamination between adjacent pixels of the differently colored QDs than the previous transfer printing approaches (Fig. 4f).

In addition to the transfer printing method, inkjet printing has also attracted significant attention since it can form the desired patterns without photo and metal-shadow masks.[103] However, the conventional inkjet printing methods are not suitable for the fine patterning of QD films because the additives used to improve the dispersion of QDs act as barriers for efficient charge transport and degrade the electrical performance of the QLEDs. However, efforts are being made to solve these issues. Recently, the Rogers group reported fine QD patterns (~5 μm) obtained using electrodynamic jet (E-jet) printing (Fig. 4g, h).[104] E-jet printing uses the electric field to eject the QD ink with a narrow width, and the resulting QD pattern shows uniform line thicknesses. Using this printing method, red and green QD pixels are formed with a resolution up to that of the commercial display.

FLEXIBLE WHITE QLEDS

White LEDs (WLEDs) are widely utilized as large-area lighting devices and/or backlight sources of the display panel. Arrays of inorganic white LEDs are being used, but point-emission, rather than areal emission, causes the areal non-uniformity. Organic white LEDs are considered as a good alternative, but many issues such as lifetime and cost still exist. Therefore, recently colloidal QDs are used as an emission component of WLEDs owing to their desirable properties, including high quantum yield, size-tunable emission spectrum, narrow emission bandwidth, and photo/thermal stability.[13–15] Considerable efforts have been devoted toward realizing highly efficient QD-based WLEDs.

First, color-converting WLEDs composed of blue/UV light sources and smaller bandgap QDs in the polymer matrix were reported.[105] Jang *et al.* reported a 46-inch TV panel using liquid crystal display with a WLED backlight by integrating red (CdSe/CdS/ZnS/CdSZnS) and green (CdSe/ZnS/CdSZnS) QDs with blue inorganic LEDs.[106] However, the color-converting WLEDs showed generally low quantum efficiencies because of the reabsorption of high-energy photons by small bandgap QDs, internal photoscattering, photobleaching, and imbalanced charge carriers. In addition, the broad emission spectra of the conventional light sources reduced the luminous efficacy and showed low color rendering index (CRI).

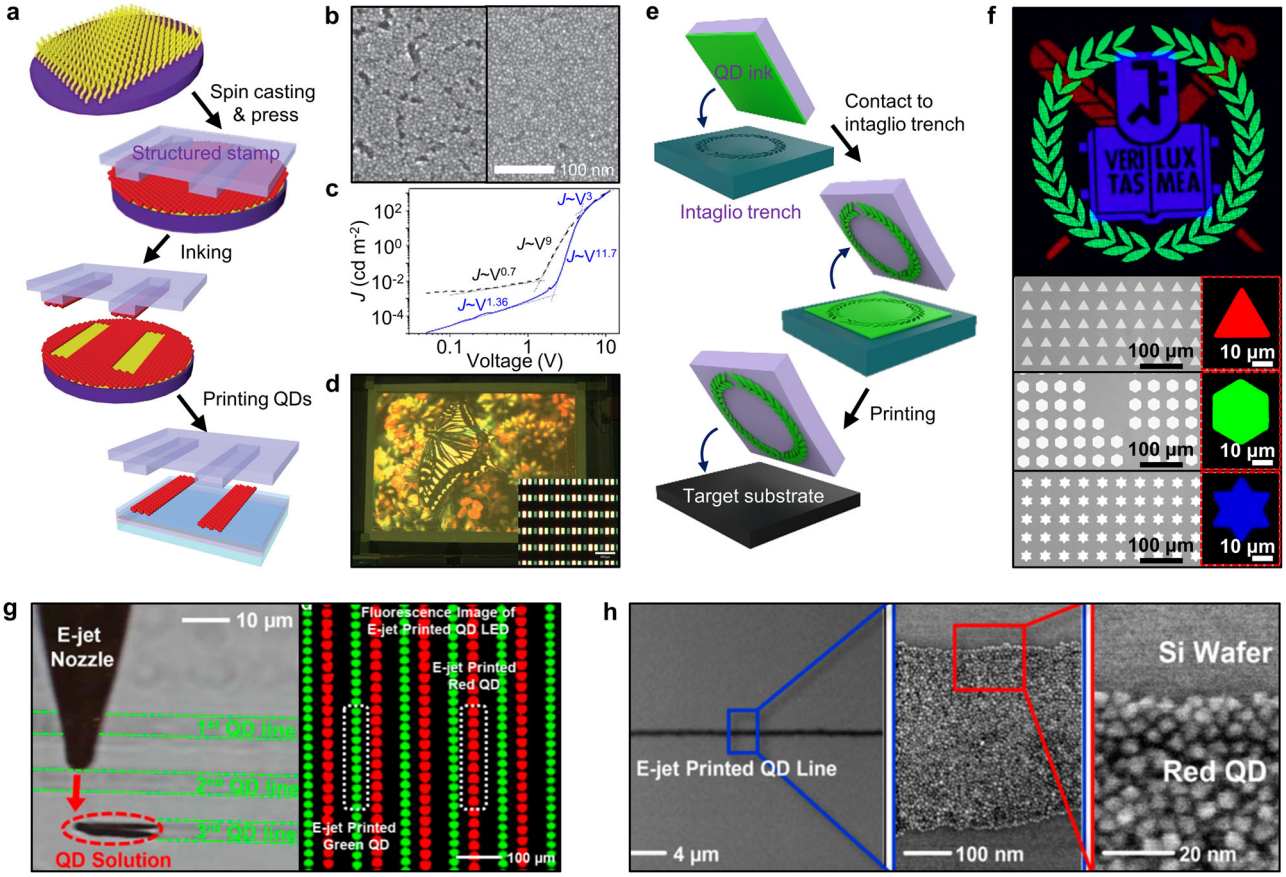

Fig. 4 Patterning techniques for multicolor QLEDs. **a** Scheme illustrating pick-and-release transfer printing using structured stamp. **b** SEM image of QD morphology before (left) and after (right) transfer printing. **c** *J–V* characteristics of QLEDs fabricated by transfer printing. **d** Four-inch full-color QD display. Inset shows the EL of transfer printed RGB pixels. **e** Scheme illustrating intaglio transfer printing. **f** Multiple transferred hierarchical RGB patterns. Bottom images show the SEM image and PL image of magnified RGB patterns. **g** Images of E-jet printing. The right image shows E-jet printed dual-color QD patterns. **h** SEM image of monolayered 400 nm line pattern. Right images show the magnified view of the E-jet printed QD line. Figure reproduced with permission from: **a**–**d** ref. [97] © 2011 NPG; **e**, **f** ref. [99] © 2015 NPG; **g**, **h** ref. [104] © 2015 ACS

To enhance the CRI and efficiency of WLEDs, EL-based white QLEDs were developed by using a mixture of QDs with different colors (Fig. 5a).[107] In 2007, the Bawendi and Bulović group reported a white EL device using a monolayer of randomly mixed QDs.[108] The EL spectrum was easily tunable by controlling the mixing ratio of RGB QDs, and the white QLED showed improved EQE and CRI of 0.36% and 81, respectively. The human eye can easily perceive light with wavelengths between 440 and 650 nm, and, therefore, tuning the emission spectra within this range improves the CRI value. Bae *et al.* controlled the emission spectrum of white QLEDs, by precisely adjusting the mixing ratio of the QDs of different colors (Fig. 5b, c).[109] A narrow bandwidth for the QD emitter (<30 nm) increases the color purity of monochromatic QD emission, but it also causes a wide spectral gap between the emission spectra of different colors and lowers the CRI value of WLEDs. To solve this issue, the number of emission peaks can be increased. This results in the more completely filled visible spectrum and a higher CRI value. The CRI value increases dramatically from 14 to 93, as the number of types of mixed QDs is increased from two (blue and yellow QD) to four (blue, cyan, yellow, and red). The white QLEDs based on randomly mixed QDs have advantages such as easy processing and cost reduction, but the inter-particle energy transfer between QDs of different colors induces low current efficiency, poor EQE, and red-shifted EL.[110] Therefore, the mixing ratio and the mixed structure of the different QDs should be precisely optimized to obtain balanced white EL.

To enhance the EL efficiency, QD monolayers stacked layer-by-layer were introduced by the SAIT group using the pick-and-place transfer-printing technique (Fig. 5d).[111] By adjusting the stacked order of the RGB QD monolayers, the nonradiative energy transfer (*e.g.*, G → R) was prevented, and true white EL could be achieved (Fig. 5e, f). However, the vertically stacked QD layers inevitably showed interparticle energy transfer[112,113] (*e.g.*, G → R or B → R) because the QD layers of different colors were stacked in the direction of charge injection. Moreover, the EL spectrum was blue-shifted as the applied bias was increased because of the increased EL contribution of the larger bandgap QDs at the higher bias condition.

The white QLED based on the pixelated RGB QD array can solve these problems (Fig. 5g–j). Recently the Kim group reported a high-resolution RGB pixel array (>2400 ppi) using the intaglio transfer-printing method (Fig. 5h, i).[99] As shown in Fig. 5j, the carrier lifetime of the pixelated QD layer and that of the blue QD layer excited at the same wavelength (440 nm) were similar, but the carrier lifetime of the RGB mixed layer was much shorter because of the Förster energy transfer between QDs in the mixed QD layer. This result shows that pixelated RGB WQLEDs are more efficient than WQLEDs using mixed QDs. If the transistors individually controlled the EL of the RGB QD pixels, the pixelated QLED would show even higher performances under various luminances.

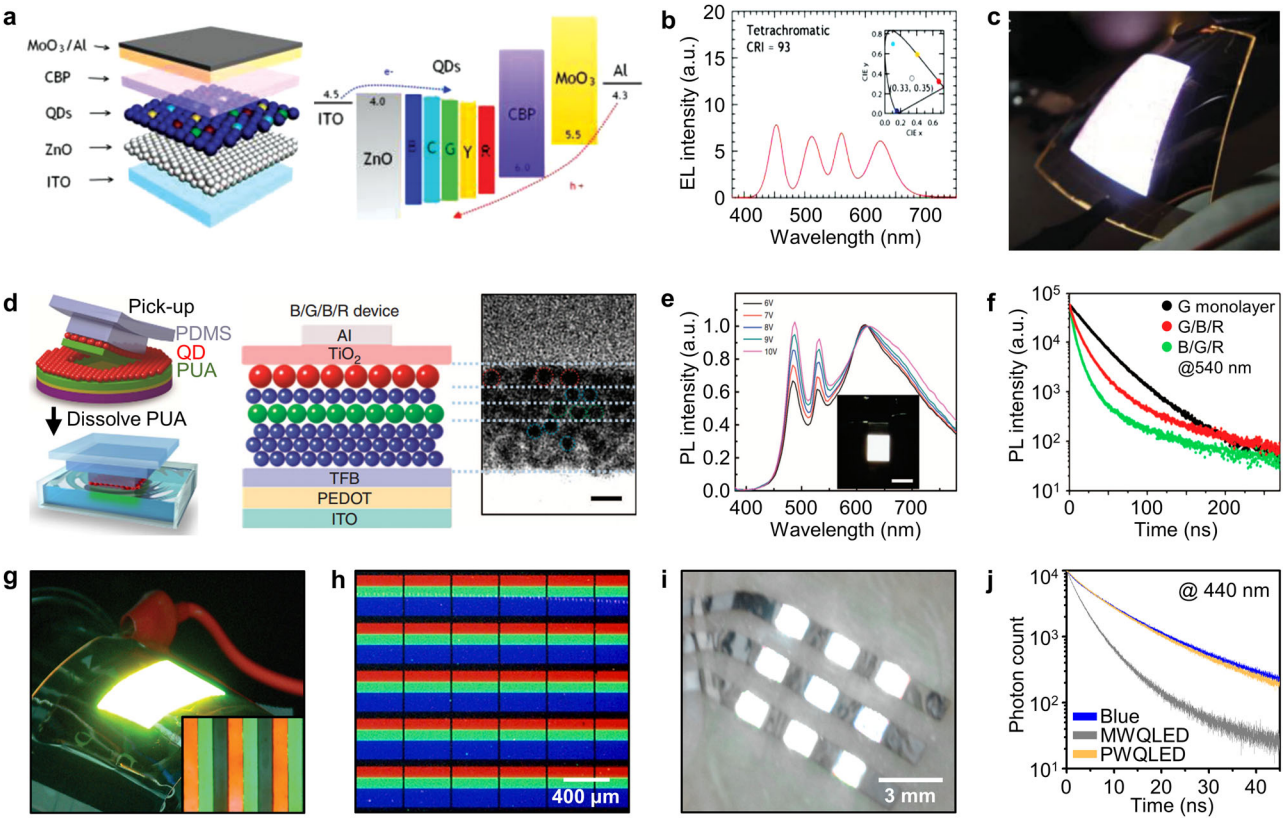

Fig. 5 Flexible white QLEDs. **a** Device structure (left) and corresponding energy diagram (right) of a white QLED with mixed RGB QD emitting layers. **b**, **c** EL of flexible white QLEDs (**b**) and corresponding EL spectra (**c**). **d** Scheme illustrating the transfer-printing process for a QD monolayer. Structure of white QLED with multiple stacked QD layers and corresponding cross-sectional TEM image. Scale bar, 10 nm. **e** PL spectrum of B/G/B/R white QLEDs under various applied voltages. **f** TRPL decay of multistacked QD films with different layer structures. **g** Flexible white QLED with RGB patterns prepared using pick-and-release transfer printing. Inset shows the RGB pixels of the white QLED. **h** RGB patterns for white QLEDs using intaglio transfer printing. **i** Ultrathin white QLED array attached to human skin. **j** TRPL spectra of a blue QD layer and white QLEDs composed of RGB pixels (pixelated white QLED; PWQLED) and mixed QD layer (MWQLED). Figure reproduced with permission from: **a**–**c** ref. [109] © 2014 Wiley; **d**–**f** ref. [111] © 2013 NPG; **g** ref. [97] © 2011 NPG; **h**–**j** ref. [99] © 2015 NPG

Table 2. Representative characteristics of transparent QLEDs

Electrode material		Transparency @ 550 nm (%)	Current efficiency (cd A^{-1})	Max. luminance (cd m^{-2})	Device lifetime	Reference
Anode	Cathode					
ITO	Ag 18 nm	55	1.25	10,540 (8.4 V)	–	[118]
ITO	Ca/Ag	45	1	500 (13 V)	–	[119]
Graphene	Graphene	75	0.45	358 (29 V)	–	[128]
ITO	Ag NWs	–	5.6	25,040 (7 V)	2 h @ 80 mA	[135]
ITO	IZO	72	0.45	200 (16 V)	–	[115]
ITO	ITO	70	3.5	9146 (15 V)	–	[136]
ITO	ITO	90	17.5	43,000 (9 V)	23.8 h @ 3.4 mA	[50]

FLEXIBLE TRANSPARENT QLEDS

Fabrication of transparent displays suitable for windows, glasses, and transparent housewares would increase the range of display applications significantly by allowing the projection of visual information onto a background without affecting its original appearance and background views.[114] In particular, flexible transparent displays enable novel curved display applications such as the smart car window, wearable smart watch, and public signage display. Until now, however, the EL performances of flexible transparent displays were significantly lower than those of their nontransparent counterparts,[115] mainly as a result of the constraints in transparent electrodes that require high conductivity, high transparency, and proper energy levels for effective charge injections simultaneously.[116] Table 2 summarizes the optical and electrical performances of previously reported transparent QLEDs including transparency, current efficiency, and device lifetime.

To achieve flexibility in transparent LEDs, thin metal films (*e.g.*, Au, Ag, Ca/Ag, and Al) have been used as the semi-transparent electrode (Fig. 6a).[117–119] Reducing the thickness of the metal film

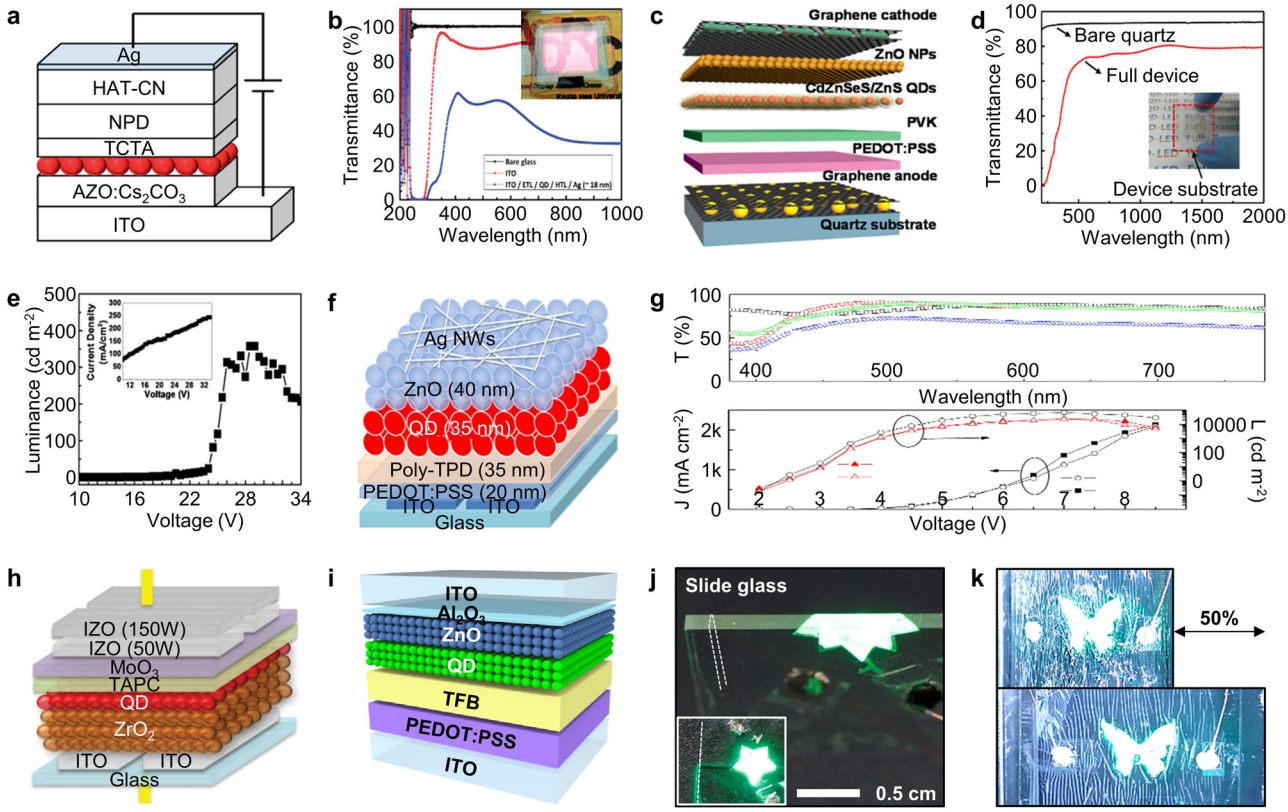

Fig. 6 Flexible transparent QLEDs. **a**, **b** Device structure (**a**) and the corresponding transparency (**b**) of semi-transparent QLEDs. Inset of (**b**) shows the EL of semitransparent QLED. **c**–**e** Exploded view (**c**), transparency (**d**), and *L*–*V* properties (**e**) of graphene based transparent QLEDs. Inset of (**e**) shows *J*–*V* properties of the same device. **f**, **g**, Device structure (**f**), transparency (**g**; top), and *J*–*V*–*L* characteristics (**g**; bottom) of Ag NWs-based transparent QLEDs. **h** Schematic representation of TCO-based transparent QLEDs with TCO buffer layers. **i** Schematic representation of ITO-based transparent QLEDs with alumina-modified ZnO ETL layer. **j**, **k** Ultrathin flexible transparent QLEDs with foldable (**j**) and stretchable (**k**) form factors. Figure reproduced with permission from: **a**, **b** ref. [118] © 2014 RSC; **c**–**e** ref. [128] © 2014 ACS; **f**, **g** ref. [135] © 2015 NPG; **h** ref. [115] © 2016 Wiley; **i**–**k** ref. [50] © 2017 Wiley

from ~100 nm to less than ~10 nm maintains the original wavelengths of light emission. However, the metal film unfortunately sacrifices the device transparency particularly when it comes to low resistance electrodes. In fact, the transparency of semi-transparent QLEDs is less than 60%, and it gets lower as the viewing angle increases (Fig. 6b). Currently, graphene is an attractive candidate material for the next generation of transparent electrodes owing to its ultrathin thickness, high transparency, and low resistance.[120–127] Seo *et al.* reported fully transparent QLEDs using Au-nanoparticle (NP)-doped graphene and Ag-nanowire (NW)-decorated graphene as anode and cathode, respectively (Fig. 6c).[128] The intercalation of Au NPs and Ag NWs into the graphene layers effectively modulates the energy level of the electrode, while maintaining the high transparency and low sheet resistance (Fig. 6d). To prevent the contamination of the underlying emitting layers, the engineered graphene electrode was formed using the dry transfer printing method instead of the conventional scooping process. However, the transferred graphene layers showed high sheet resistance because of the high contact resistance, which consequently decreased the EL properties of the QLEDs, including the high turn-on voltage and low brightness (Fig. 6e).

Ag NWs represent another good candidate for transparent electrodes.[129–132] The percolated assembly of ultralong Ag NWs provides low sheet resistance (<10 Ω sq^{-1}),[133,134] while maintaining high transparency owing to their highly porous structure. As Ag NWs are easily deposited on the target surface by spin casting or doctor blading, the Ag NW-based QLEDs can be cost-effective and highly flexible. For instance, the Zhang group reported solution-processed transparent QLEDs with an Ag NW cathode, which showed high luminance (~25,000 cd m^{-2}) and high transparency (70%) (Fig. 6f, g).[135] Although graphene and Ag NWs have shown meaningful advances, their device performances need to be improved further.

Transparent-conducting oxides (TCOs) have been the most widely utilized transparent electrodes over the past decades. However, the fabrication of TCO-based transparent top electrode remains challenging because of the mechanical and/or chemical damages to the underlying emitting materials during the harsh deposition process (*e.g.*, sputtering).[136] Pre-deposition of the thick inorganic buffer layers and successive sputtering process of the top TCO electrode have been employed to prevent the damages to the QD layer and formation of unwanted conducting paths between CTLs (Fig. 6h).[115] However, the transparent light-emitting devices still show low EL characteristics compared with the nontransparent counterparts because of imbalanced charge carriers within the devices. Moreover, the thick ETL and/or inorganic buffer layers increase the stiffness, thereby decreasing the flexibility of the QLEDs. In 2017, the Kim group reported the engineered ETL structure composed of ZnO NPs and ultrathin alumina overlayers (Fig. 6i).[50] Modification of inorganic ETL structure with the 2 nm-thick alumina overlayer effectively protected the emitting layer and balanced electron/hole injection into QDs, thus resulting in highly transparent (84% over visible range) and bright (~43,000 cd m^{-2}) QLEDs. They also reported foldable and stretchable transparent QLEDs, prepared using the parylene-epoxy double layer as encapsulation and the buckled device structure (Fig. 6j, k). The ultrathin flexible transparent

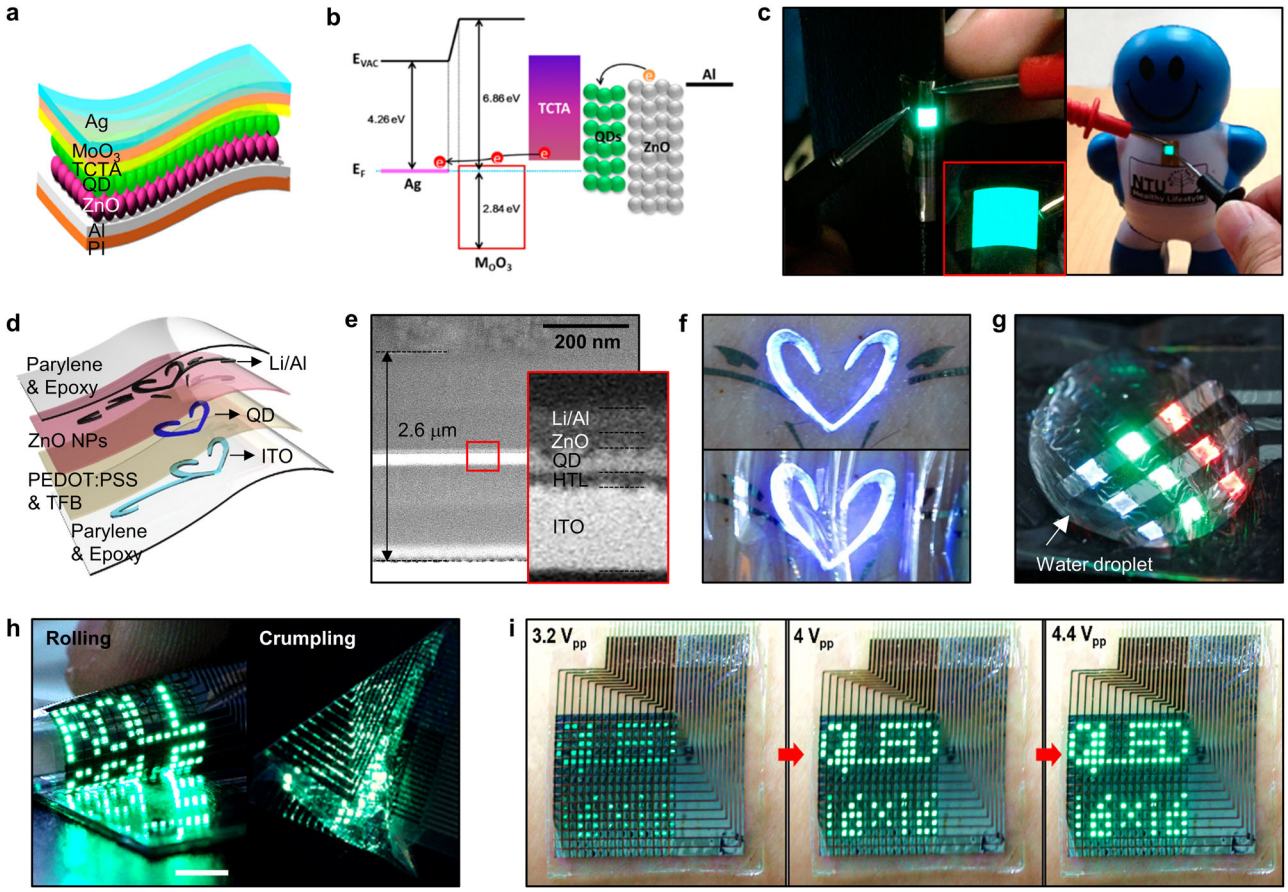

Fig. 7 Wearable quantum dot display. **a**, **b** Schematic illustration (**a**) and energy diagram (**b**) of the sticker-type top-emission QLED film. **c** Curved QLEDs on the edge of a thin steel plate (left) and on curvilinear surface of a toy (right). Inset of the left image shows a large-area QLED on a flexible substrate (20 mm × 25 mm). **d**, **e** Schematic illustration (**d**) and cross-sectional SEM image (**e**) of the tattoo-like wearable QLED. Inset of (**e**) shows the magnified device structure. **f** Ultrathin tattoo-like QLEDs laminated on human arm. **g** Waterproof properties of ultrathin QLEDs. **h** Ultrathin QLED display (left: rolling, right: crumpling). **i** Sequential images of the QLED display with different operating voltages. Figure reproduced with permission from: **a**–**c** ref. [149] © 2014 ACS; **d**–**g** ref. [99] © 2015 NPG; **h**, **i** ref. [51] © 2017 Wiley

QLEDs showed highly stable EL during 1000 cycles of the bending test because the designed ETL layer did not increase the overall thickness of the QLEDs, and fragile ITO electrodes were located in the pseudo-neutral mechanical plain. These ultrathin and flexible transparent QLEDs can be incorporated onto the surface of a variety of curved objects, which can be a step forward to a smart Internet of things (IoTs).

WEARABLE QUANTUM DOT DISPLAYS

One of the most promising applications of flexible QLEDs is the wearable display. Skin-mounted electronics have provided new routes for advanced wearable diagnostic/therapeutic solutions.[137–146] However, significant challenges still remain for the wearable displays that can show the monitored data from the wearable sensors to the user in real time. One of the major challenges for ideal wearability is the thickness and stiffness of the conventional flexible displays.[147] The high water/air stability of QLEDs enables a much thinner encapsulation layer compared to organic LEDs, which increases the flexibility of the device dramatically.

Flexible QLEDs have been commonly manufactured based on ITO electrodes patterned on a flexible PET substrate, whose thickness was in the range of hundreds of micrometers.[148] Owing to the thick substrate and the fragile ITO electrode, the minimum bending radius of the display was limited to several tens of millimeters. For highly flexible QLEDs, the Demir group reported a sticker-like top-emitting QLED using a Kapton polyimide film as a substrate and a thin metal film as a semitransparent electrode (Fig. 7a, b).[149] The high stability of the polyimide film against thermal/solvent exposure enabled high-temperature annealing during QLED fabrication, and the thin Ag electrode (18 nm) acted as a semitransparent top electrode, which could endure mechanical deformations. The thin-film–type QLED was easily deformed and laminated on curved surfaces of various objects, including the edge of a thin plate and the chest of a mascot doll (Fig. 7c).

For wearable displays, it is essential to establish a biocompatible ultrathin encapsulation layer. Choi *et al.* reported parylene-epoxy double-layered ultrathin QLEDs for electronic tattoo-like displays (Fig. 7d).[99] The FDA (Food and Drug Administration) approved biocompatible parylene-C film forms a good interface with skin and protects it from rashes or itching. The ultrathin epoxy layer also prevents any damage to the parylene film during the sputtering process of the bottom ITO electrode. The thickness of the double-layered encapsulation is ~1.2 μm, and the overall thickness of the QLED is ~2.6 μm (Fig. 7e). As the fragile ITO electrode is located near the neutral mechanical plane, where tensile and compressive strains are compensated, the ultrathin QLED can be freely deformed without mechanical fractures, even on soft human skin (Fig. 7f). Even in the wavy deformed state with a radius of curvature of the micrometer scale, the peak strain applied to the flexible QLED is less than the fracture strain of ITO electrode (~2.2%), that allows highly deformable flexible QLED.[50] In addition, the ultrathin encapsulation layer makes the device

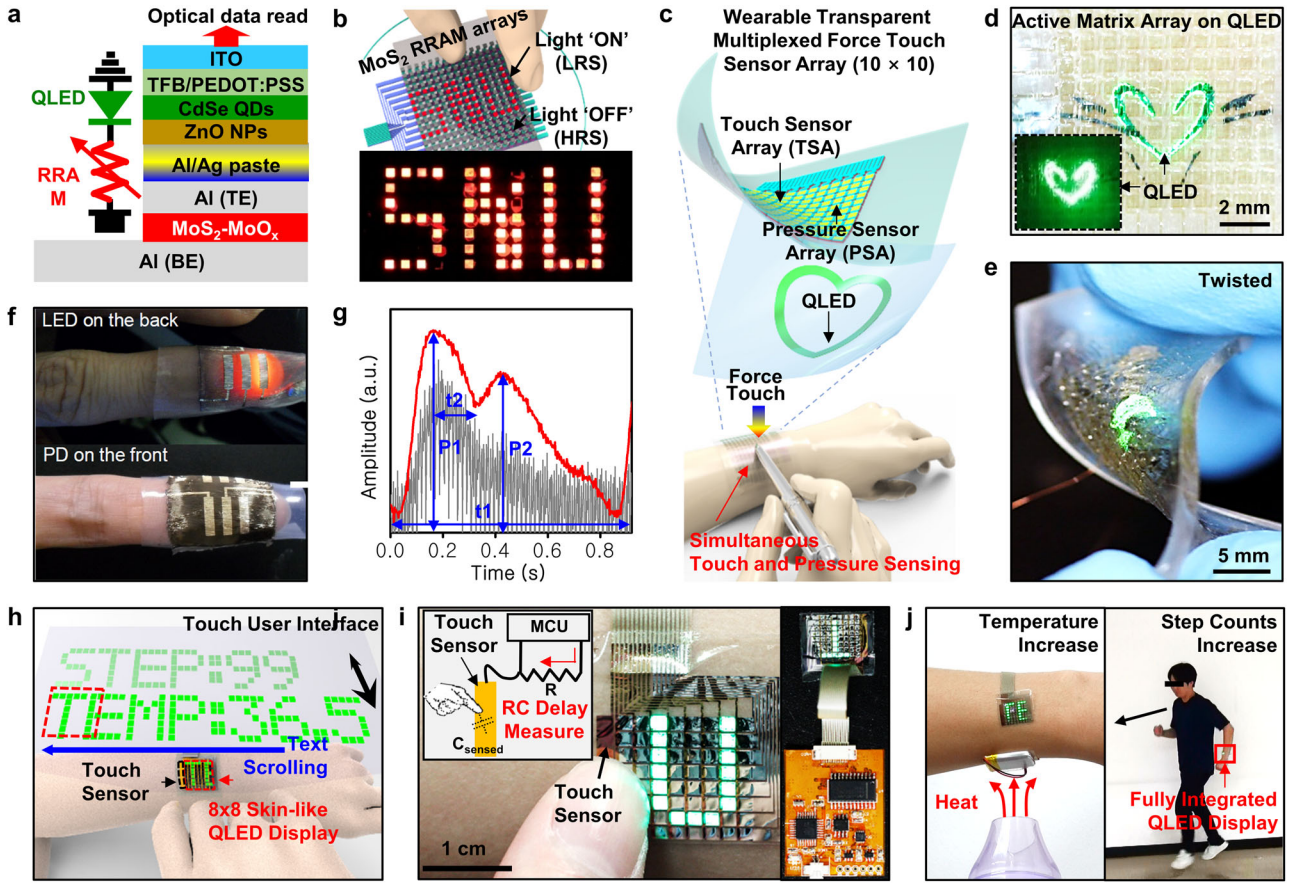

Fig. 8 Wearable QLEDs integrated with other electronic devices. **a**, **b** Cross-sectional device structure (**a**) and schematic illustration (**b**) of the QLED display integrated with MoS_2 ReRAM. **c**, **d** Schematic representation (**c**) and image (**d**) of transparent and wearable force touch sensor array integrated with a skin-mounted QLED. Inset of (**d**) shows the QLEDs under dark conditions. **e** Twisted wearable devices on ultrathin QLEDs. **f** Epidermal PPG sensor composed of QLED and QD PD. **g** PPG signal from the QD-based epidermal PPG sensor. **h**, **i** Schematic illustration (**h**) and photograph (**i**) of the ultrathin QLED display integrated with wearable electronics. Inset of (**i**) shows an illustration of the measurement setup. **j** Integrated wearable electronic system subjected to external heat (left) and running wearer (right). Skin-mounted QLED shows the measured information. Figure reproduced with permission from: **a**, **b** ref. [155] © 2016 Wiley; **c**–**e** ref. [156] © 2017 Wiley; **f**, **g** ref. [158] © 2017 ACS; **h**–**j** ref. [51] © 2017 Wiley

waterproof, which effectively protects the wearable QLED under high humidity conditions (Fig. 7g). By applying a passive matrix array design, the wearable QLED displays diverse information even in rolled and crumpled objects (Fig. 7h).[51] Figure 7i shows sequential images displayed on the epidermal QLED. The passively operating wearable QLEDs minimize power consumption and suppress overheating owing to the line-by-line passive matrix operation process, which ensures the safe operation of the wearable display on human skin.

FLEXIBLE QLEDS INTEGRATED WITH OTHER ELECTRONIC DEVICES

In this section, we discuss flexible QLEDs integrated with other electronic components such as sensors, memories, controllers, and Bluetooth units for the next-generation portable and/or wearable type of electronic/optoelectronic systems.[150–154] The flexible form factor of the integrated electronic system will provide new design platform for the wearable display.

One interesting application based on flexible QLEDs is a smart pressure-sensitive display, which measures, stores, and displays external mechanical deformations in real time. Son *et al.* integrated MoS_2-based resistive random-access memory (ReRAM) devices and pressure sensors with a QLED array.[155] The measured data from the pressure sensor were first stored in the MoS_2 ReRAM array, and subsequently the written data were displayed visually through the QLED array (Fig. 8a, b). The wearable QLEDs could be integrated with a multiplexed transparent touch sensor array as an input port of user's intentions (Fig. 8c). The ultrathin QLED can be also integrated with transparent force touch sensors (i.e., pressure sensors and touch sensors) (Fig. 8d).[156] The soft integrated electronic system could be laminated on the human skin by van der Waals force alone, and operated stably even in the deformed state (Fig. 8e). These system-level integration examples confirm the possibility of novel wearable electronic systems integrated with wearable displays.

The wearable QLED, i.e., another application example of the flexible QLED, can work as a light source for wearable light-based biosensors.[157] In 2017, Kim *et al.* reported wearable photoplethysmographic (PPG) sensors that combined stretchable QLEDs and QD photodetectors.[158] The graphene-based transparent electrode provided extreme bendability for the QD-based LEDs and PDs. The QLED was transferred onto a prestrained elastomer to form a buckled structure, and displayed 70% stretchability. For the PPG sensors, the stretchable QLEDs and PDs were attached around the fingertip, side by side, and performed as a light source and detector, respectively (Fig. 8f). The absorption spectrum changes could be well correlated with the pulse. The wearable PPG sensor also measured accurately fine changes in pressure (Fig. 8g). Such an optoelectronic device composed of QD-based LEDs and PDs

can be utilized for diverse wearable sensor applications such as human motion detection and/or heart rate measurement.

Another application example of QLEDs in fully integrated wearable electronics is a flexible printed circuit board (FPCB), which integrates the QLED display, touch sensors, microcontroller modules, wireless units, other physical sensors, and power sources (Fig. 8h–j).[51] The touch sensor is co-embedded with a QLED display, while maintaining an ultrathin form factor (5.5 μm). The touch interface provides an interactive user interface by changing the sensing mode in the QLED display (Fig. 8i). The 8×8 ultrathin QLED passive matrix array laminated on the human arm can display temperature and step information measured from the wearable sensors (Fig. 8i, right) in real time (Fig. 8j). This fully integrated wearable QLED display can provide new insights for advanced wearable healthcare electronic systems.

CONCLUSIONS

In this review, we discussed the recent developments and cutting-edge technologies in flexible and wearable QLEDs. Tremendous efforts have been made to improve the EL performance of QLEDs by optimizing device structures and QD synthetic methods. Despite several challenges (*e.g.*, long-term device lifetime, low EL efficiencies for blue emissions, toxicity of Cd-based QDs), QLEDs exhibit unique characteristics that surpass other types of LEDs, such as high color purity, high brightness with low turn-on voltage, high resolution RGB array patterning, and ultrathin form factors. These advantages make QLEDs promising for the next-generation display applications, particularly in the field of flexible/wearable electronics. Recent advances in QD processing, encapsulation technology, and unconventional device/system designs have resulted in even faster development of flexible QLEDs. With these technological progresses, QLEDs can be successfully applied to more advanced devices such as flexible white QLEDs and highly transparent flexible QLEDs. Each key technology of unconventional QLEDs provide many opportunities in novel electronics and optoelectronics. It has been recently demonstrated that these QLEDs can be successfully integrated with various wearable electronic devices, including wearable sensors, data storage modules, touch interfaces, and flexible wireless data transfer devices for fully integrated systems. In the future, other home applications and mobile electronics will be connected wirelessly and wearable displays will visualize information for users. These technological advances shed light on the promising future of flexible QLEDs and related next-generation displays.

Data availability

The data that support the findings of this study are available from the corresponding author on request.

ACKNOWLEDGEMENTS

This research was supported by IBS-R006-D1 and IBS-R006-A1.

AUTHOR CONTRIBUTIONS

All authors contributed to this manuscript.

ADDITIONAL INFORMATION

Competing interests: The authors declare no competing interests.

Publisher's note: Springer Nature remains neutral with regard to jurisdictional claims in published maps and institutional affiliations.

REFERENCES

1. Kim, J., Ghaffari, R. & Kim, D.-H. The quest for miniaturized soft bioelectronics devices. *Nat. Biomed. Eng.* **1**, 0049 (2017).
2. Son, D. et al. Stretchable carbon nanotube charge-trap floating-gate memory and logic devices for wearable electronics. *ACS Nano* **9**, 5585–5593 (2015).
3. Yokota, T. et al. Ultraflexible organic photonic skin. *Sci. Adv.* **2**, e1501856 (2016).
4. Sekitani, T. et al. Stretchable active-matrix organic light-emitting diode display using printable elastic conductors. *Nat. Mater.* **8**, 494–499 (2009).
5. White, M. S. et al. Ultrathin, highly flexible and stretchable PLEDs. *Nat. Photon.* **7**, 811–816 (2013).
6. Son, D. et al. Multifunctional wearable devices for diagnosis and therapy of movement disorders. *Nat. Nanotechnol.* **9**, 397–404 (2014).
7. Kim, J. et al. Stretchable silicon nanoribbon electronics for skin prosthesis. *Nat. Commun.* **5**, 5747 (2014).
8. Choi, S. et al. Recent advances in flexible and stretchable bio-electronic devices integrated with nanomaterials. *Adv. Mater.* **28**, 4203–4218 (2016).
9. Kim, R.-H. et al. Waterproof AlInGaP optoelectronics on stretchable substrates with applications in biomedicine and robotics. *Nat. Mater.* **9**, 929–937 (2010).
10. Park, S.-I. et al. Printed assemblies of ultrathin, microscale inorganic light emitting diodes for deformable and semitransparent displays. *Science* **325**, 977–981 (2009).
11. Han, T.-H. et al. Extremely efficient flexible organic light-emitting diodes with modified graphene anode. *Nat. Photon.* **6**, 105–110 (2012).
12. Liang, J., Li, L., Niu, X., Yu, Z. & Pei, Q. Elastomeric polymer light-emitting devices and displays. *Nat. Photon.* **7**, 817–824 (2013).
13. Yang, J., Choi, M. K., Kim, D.-H. & Hyeon, T. Designed assembly and integration of colloidal nanocrystals for device applications. *Adv. Mater.* **28**, 1176–1207 (2016).
14. Dai, X., Deng, Y., Peng, X. & Jin, Y. Quantum-dot light-emitting diodes for large-area displays: towards the dawn of commercialization. *Adv. Mater.* **29**, 1607022 (2017).
15. Pimputkar, S., Speck, J. S., Denbaars, S. P. & Nakamura, S. Prospects for LED lighting. *Nat. Photon.* **3**, 180–182 (2009).
16. Murray, C. B., Norris, D. J. & Bawendi, M. G. Synthesis and characterization of nearly monodisperse CdE (E = sulfur, selenium, tellurium) semiconductor nanocrystallites. *J. Am. Chem. Soc.* **115**, 8706–8715 (1993).
17. Alivisatos, A. P. Semiconductor clusters, nanocrystals, and quantum dots. *Science* **271**, 933–937 (1996).
18. Yu, H., Li, J., Loomis, R. A., Wang, L. W. & Buhro, W. E. Two- versus three-dimensional quantum confinement in indium phosphide wires and dots. *Nat. Mater.* **2**, 517–520 (2003).
19. Yang, J. et al. Advances in the colloidal synthesis of two-dimensional semiconductor nanoribbons. *Chem. Mater.* **25**, 1190–1198 (2013).
20. Norris, D. J., Efros, A. L., Rosen, M. & Bawendi, M. G. Size dependence of exciton fine structure in CdSe quantum dots. *Phys. Rev. B* **53**, 16347–16354 (1996).
21. Ithurria, S. et al. Colloidal nanoplatelets with two-dimensional electronic structure. *Nat. Mater.* **10**, 936–941 (2011).
22. Son, J. S. et al. Dimension-controlled synthesis of CdS nanocrystals: from 0D quantum dots to 2D nanoplates. *Small* **8**, 2394–2402 (2012).
23. Yang, J. et al. Route to the smallest doped semiconductor: Mn^{2+}-doped $(CdSe)_{13}$ clusters. *J. Am. Chem. Soc.* **137**, 12776–12779 (2015).
24. Kagan, C. R., Lifshitz, E., Sargent, E. H. & Talapin, D. V. Building devices from colloidal quantum dots. *Science* **353**, aac5523 (2016).
25. Goesmann, H. & Feldmann, C. Nanoparticulate functional materials. *Angew. Chem. Int. Ed.* **49**, 1362–1395 (2010).
26. Wood, V. & Bulovic´, V. Colloidal quantum dot light-emitting devices. *Nano Rev.* **1**, 1–7 (2010).
27. Rogach, A. L., Eychmüller, A., Hickey, S. G. & Kershaw, S. V. Infrared-emitting colloidal nanocrystals: synthesis, assembly, spectroscopy, and applications. *Small* **3**, 536–557 (2007).
28. Tessler, N., Medvedev, V., Kazes, M., Kan, S. & Banin, U. Efficient near-infrared polymer nanocrystal light-emitting diodes. *Science* **295**, 1506–1508 (2002).
29. Bakueva, L. et al. Size-tunable infrared (1000–1600 nm) electroluminescence from PbS quantum-dot nanocrystals in a semiconducting polymer. *Appl. Phys. Lett.* **82**, 2895–2897 (2003).
30. Yang, J. et al. Copper–indium–selenide quantum dot-sensitized solar cells. *Phys. Chem. Chem. Phys.* **15**, 20517–20525 (2013).
31. Supran, G. J. et al. High-performance shortwave-infrared light-emitting devices using core-shell (PbS-CdS) colloidal quantum dots. *Adv. Mater.* **27**, 1437–1442 (2015).
32. Muckel, F. et al. Digital doping in magic-sized CdSe clusters. *ACS Nano* **10**, 7135–7141 (2016).
33. Gong, X. et al. Highly efficient quantum dot near-infrared light-emitting diodes. *Nat. Photon.* **10**, 253–257 (2016).
34. Yang, J. et al. Chemical synthesis, doping, and transformation of magic-sized semiconductor alloy nanoclusters. *J. Am. Chem. Soc.* **139**, 6761–6770 (2017).

35. Talapin, D. V., Lee, J.-S., Kovalenko, M. V. & Shevchenko, E. V. Prospects of colloidal nanocrystals for electronic and optoelectronic applications. *Chem. Rev.* **110**, 389–458 (2010).
36. Shirasaki, Y., Supran, G. J., Bawendi, M. G. & Bulovic´, V. Emergence of colloidal quantum-dot lightemitting technologies. *Nat. Photon.* **7**, 13–23 (2013).
37. Chen, Z., Nadal, B., Mahler, B., Aubin, H. & Dubertret, B. Quasi-2D colloidal semiconductor nanoplatelets for narrow electroluminescence. *Adv. Funct. Mater.* **24**, 295–302 (2014).
38. Hines, M. A. & Guyot-sionnest, P. Synthesis and characterization of strongly luminescing ZnS-capped CdSe nanocrystals. *J. Phys. Chem.* **100**, 468–471 (1996).
39. Dabbousi, B. O. et al. (CdSe)ZnS core-shell quantum dots: synthesis and characterization of a size series of highly luminescent nanocrystallites. *J. Phys. Chem. B* **101**, 9463–9475 (1997).
40. Peng, X., Schlamp, M. C., Kadavanich, A. V. & Alivisatos, A. P. Epitaxial growth of highly luminescent CdSe/CdS core/shell nanocrystals with photostability and electronic accessibility. *J. Am. Chem. Soc.* **119**, 7019–7029 (1997).
41. Bae, W. K., Char, K., Hur, H. & Lee, S. Single-step synthesis of quantum dots with chemical composition gradients. *Chem. Mater.* **20**, 531–539 (2008).
42. Lee, J., Yang, J., Kwon, S. G. & Hyeon, T. Nonclassical nucleation and growth of inorganic nanoparticles. *Nat. Rev. Mater.* **1**, 16034 (2016).
43. Owen, J. & Brus, L. Chemical synthesis and luminescence applications of colloidal semiconductor quantum sots. *J. Am. Chem. Soc.* **139**, 10939–10943 (2017).
44. Mahler, B. et al. Towards non-blinking colloidal quantum dots. *Nat. Mater.* **7**, 659–664 (2008).
45. Chen, Y. et al. 'Giant' multishell CdSe nanocrystal quantum dots with suppressed blinking. *J. Am. Chem. Soc.* **130**, 5026–5027 (2008).
46. Galland, C. et al. Lifetime blinking in nonblinking nanocrystal quantum dots. *Nat. Commun.* **3**, 908 (2012).
47. Bae, W. K. et al. Controlling the influence of Auger recombination on the performance of quantum-dot light-emitting diodes. *Nat. Commun.* **4**, 2661 (2013).
48. Lim, J. et al. Influence of shell thickness on the performance of light-emitting devices based on CdSe/Zn1-XCdXS core/shell heterostructured quantum dots. *Adv. Mater.* **26**, 8034–8040 (2014).
49. Lee, K.-H. et al. Over 40 cd/A efficient green quantum dot electroluminescent device comprising uniquely large-sized quantum dots. *ACS Nano* **8**, 4893–4901 (2014).
50. Choi, M. K. et al. Extremely vivid, highly transparent, and ultrathin quantum dot light-emitting diodes. *Adv. Mater.* **30**, 1703279 (2018).
51. Kim, J. et al. Ultrathin quantum dot display integrated with wearable electronics. *Adv. Mater.* **29**, 1700217 (2017).
52. Yang, Y. et al. High-efficiency light-emitting devices based on quantum dots with tailored nanostructures. *Nat. Photon.* **9**, 259–266 (2015).
53. Oh, N. et al. Double-heterojunction nanorods. *Nat. Commun.* **5**, 3642 (2014).
54. Nam, S., Oh, N., Zhai, Y. & Shim, M. High efficiency and optical anisotropy in double-heterojunction nanorod light-emitting diodes. *ACS Nano* **9**, 878–885 (2015).
55. Oh, N. et al. Double-heterojunction nanorod light-responsive LEDs for display applications. *Science* **355**, 616–619 (2017).
56. Choi, H. S. et al. Renal clearance of quantum dots. *Nat. Biotechnol.* **25**, 1165–1170 (2007).
57. Pons, T. et al. Cadmium-free CuInS2/ZnS quantum dots for sentinel lymph node imaging with reduced toxicity. *ACS Nano* **4**, 2531–2538 (2010).
58. Yu, J. H. et al. High-resolution three-photon biomedical imaging using doped ZnS nanocrystals. *Nat. Mater.* **12**, 359–366 (2013).
59. Kim, J.-Y. et al. Highly efficient copper–indium–selenide quantum dot solar cells: suppression of carrier recombination by controlled ZnS overlayers. *ACS Nano* **9**, 11286–11295 (2015).
60. Du, J. et al. Zn–Cu–In–Se quantum dot solar cells with a certified power conversion efficiency of 11.6%. *J. Am. Chem. Soc.* **138**, 4201–4209 (2016).
61. Xu, G. et al. New generation cadmium-free quantum dots for biophotonics and nanomedicine. *Chem. Rev.* **116**, 12234–12327 (2016).
62. Oh, E. et al. Meta-analysis of cellular toxicity for cadmium-containing quantum dots. *Nat. Nanotechnol.* **11**, 479–486 (2016).
63. Xie, R., Battaglia, D. & Peng, X. G. Colloidal InP nanocrystals as efficient emitters covering blue to near-infrared. *J. Am. Chem. Soc.* **129**, 15432–15433 (2007).
64. Li, L. & Reiss, P. One-pot synthesis of highly luminescent InP/ZnS nanocrystals without precursor injection. *J. Am. Chem. Soc.* **130**, 11588–11589 (2008).
65. Tamang, S., Lincheneau, C., Hermans, Y., Jeong, S. & Reiss, P. Chemistry of InP nanocrystal syntheses. *Chem. Mater.* **28**, 2491–2506 (2016).
66. Bang, E. et al. Large-scale synthesis of highly luminescent InP@ZnS quantum dots using elemental phosphorus precursor. *Chem. Mater.* **29**, 4236–4243 (2017).
67. Lim, J. et al. InP@ZnSeS, core@composition gradient shell quantum dots with enhanced stability. *Chem. Mater.* **23**, 4459–4463 (2011).
68. Kim, S. et al. Highly luminescent InP/GaP/ZnS nanocrystals and their application to white light-emitting diodes. *J. Am. Chem. Soc.* **134**, 3804–3809 (2012).
69. Lim, J. et al. Highly efficient cadmium-free quantum dot light-emitting diodes enabled by the direct formation of excitons within InP@ZnSeS quantum dots. *ACS Nano* **7**, 9019–9026 (2013).
70. Wang, C. W. et al. Cadmium-free InP/ZnSeS/ZnS heterostructure-based quantum dot light-emitting diodes with a ZnMgO electron transport layer and a brightness of over 10,000 cd m^{-2}. *Small* **13**, 1603962 (2017).
71. Zhang, Y. et al. Employing heavy metal-free colloidal quantum dots in solution-processed white light-emitting diodes. *Nano. Lett.* **11**, 329–332 (2011).
72. Tan, Z. et al. Near-band-edge electroluminescence from heavy-metal-free colloidal quantum dots. *Adv. Mater.* **23**, 3553–3558 (2011).
73. Kim, J.-H. & Yang, H. High-efficiency Cu−In−S quantum-dot-light-emitting device exceeding 7%. *Chem. Mater.* **28**, 6329 (2016).
74. Wepfer, S. et al. Solution-processed CuInS2-based white QD-LEDs with mixed active layer architecture. *ACS Appl. Mater. Interfaces* **9**, 11224–11230 (2017).
75. Knowles et al. Luminescent colloidal semiconductor nanocrystals containing copper: synthesis, photophysics, and applications. *Chem. Rev.* **116**, 10820–10851 (2016).
76. Colvin, V. L., Schlamp, M. C. & Alivisatos, A. P. Light-emitting diodes made from cadmium selenide nanocrystals and a semiconducting polymer. *Nature* **370**, 354–357 (1994).
77. Schlamp, M. C., Peng, X. & Alivisatos, A. P. Improved efficiencies in light emitting diodes made with CdSe(CdS) core/shell type nanocrystals and a semiconducting polymer. *J. Appl. Phys.* **82**, 5837 (1997).
78. Mattoussi, H. et al. Electroluminescence from heterostructures of polyphenylene vinylene and inorganic CdSe nanocrystals. *J. Appl. Phys.* **83**, 7965 (1998).
79. Coe, S., Woo, W.-K., Bawendi, M. & Bulovic, V. Electroluminescence from single monolayers of nanocrystals in molecular organic devices. *Nature* **420**, 800–803 (2002).
80. Coe-Sullivan, S., Steckel, J. S., Woo, W.-K., Bawendi, M. G. & Bulovic, V. Large-area ordered quantum-dot monolayers via phase separation during spin-casting. *Adv. Funct. Mater.* **15**, 1117–1124 (2005).
81. Zhao, J. et al. Efficient CdSe/CdS quantum dot light-emitting diodes using a thermally polymerized hole transport layer. *Nano Lett.* **6**, 463–467 (2006).
82. Niu, Y. H. et al. Improved performance from multilayer quantum dot light-emitting diodes via thermal annealing of the quantum dot layer. *Adv. Mater.* **19**, 3371–3376 (2007).
83. Jing, P. et al. Shell-dependent electroluminescence from colloidal CdSe quantum dots in multilayer light-emitting diodes. *J. Appl. Phys.* **105**, 044313 (2009).
84. Castelli, A. et al. High-efficiency all-solution-processed light-emitting diodes based on anisotropic colloidal heterostructures with polar polymer injecting layers. *Nano Lett.* **15**, 5455–5464 (2015).
85. Mueller, A. H. et al. Multicolor light-emitting diodes based on semiconductor nanocrystals encapsulated in GaN charge injection layers. *Nano Lett.* **5**, 1039–1044 (2005).
86. Caruge, J. M., Halpert, J. E., Bulovic, V. & Bawendi, M. G. Colloidal quantum-dot light-emitting diodes with metal-oxide charge transport layers. *Nat. Photon.* **2**, 247–250 (2008).
87. Wood, V. et al. Selection of metal oxide charge transport layers for colloidal quantum dot LEDs. *ACS Nano* **3**, 3581–3586 (2009).
88. Bendall, J. S. et al. Layer-by-layer all-inorganic quantum-dot-based LEDs: a simple procedure with robust performance. *Adv. Funct. Mater.* **20**, 3298–3302 (2010).
89. Caruge, J.-M., Halpert, J. E., Bulovic, V. & Bawendi, M. G. NiO as an inorganic hole-transporting layer in quantum-dot light-emitting devices. *Nano Lett.* **6**, 2991–2994 (2006).
90. Stouwdam, J. W. & Janssen, R. A. J. Red, green, and blue quantum dot LEDs with solution processable ZnO nanocrystal electron injection layers. *J. Mater. Chem.* **18**, 1889–1894 (2008).
91. Cho, K. S. et al. High-performance crosslinked colloidal quantum-dot light-emitting diodes. *Nat. Photon.* **3**, 341–345 (2009).
92. Kazlas, P. T. et al. Quantum dot light emitting diodes for full-color active-matrix displays. *SID Symp. Dig. Tech. Pap.* **41**, 473–476 (2010).
93. Qian, L., Zheng, Y., Xue, J. & Holloway, P. H. Stable and efficient quantum-dot light-emitting diodes based on solution-processed multilayer structures. *Nat. Photon.* **5**, 543–548 (2011).
94. Kwak, J. et al. Bright and efficient full-color colloidal quantum dot light-emitting diodes using an inverted device structure. *Nano Lett.* **12**, 2362–2366 (2012).
95. Mashford, B. S. et al. High-efficiency quantum-dot light-emitting devices with enhanced charge injection. *Nat. Photon.* **7**, 407–412 (2013).
96. Dai, X. et al. Solution-processed, high-performance light-emitting diodes based on quantum dots. *Nature* **515**, 96–99 (2014).
97. Kim, T.-H. et al. Full-colour quantum dot displays fabricated by transfer printing. *Nat. Photon.* **5**, 176–182 (2011).
98. Shen, H. et al. High-efficiency, low turn-on voltage blue-violet quantum-dot-based light-emitting diodes. *Nano Lett.* **15**, 1211–1216 (2015).

99. Choi, M. K. et al. Wearable red–green–blue quantum dot light-emitting diode array using high-resolution intaglio transfer printing. *Nat. Commun.* **6**, 7149 (2015).
100. Rizzo, A. et al. Hybrid light-emitting diodes from microcontact-printing double-transfer of colloidal semiconductor CdSe/ZnS quantum dots onto organic layers. *Adv. Mater.* **20**, 1886–1891 (2008).
101. Haverinen, H. M., Myllyla, R. A. & Jabbour, G. E. Inkjet printed RGB quantum dot-hybrid LED. *J. Disp. Technol.* **6**, 87–89 (2010).
102. Kim, L. et al. Contact printing of quantum dot light-emitting devices. *Nano Lett.* **8**, 4513–4517 (2008).
103. Wood, V. et al. Inkjet-printed quantum dot–polymer composites for full-color AC-driven displays. *Adv. Mater.* **21**, 1–5 (2009).
104. Kim, B. H. et al. High-resolution patterns of quantum dots formed by electrohydrodynamic jet printing for light-emitting diodes. *Nano Lett.* **15**, 969–973 (2015).
105. Jang, H. S. et al. White light-emitting diodes with excellent color rendering based on organically capped CdSe quantum dots and Sr_3SiO_5:Ce^{3+},Li^{+} phosphors. *Adv. Mater.* **20**, 2696–2702 (2008).
106. Jang, E. et al. White-light-emitting diodes with quantum dot color converters for display backlights. *Adv. Mater.* **22**, 3076–3080 (2010).
107. Lee, K.-H. et al. Highly efficient, color-reproducible full-color electroluminescent devices based on red/green/blue quantum dot-mixed multilayer. *ACS Nano* **9**, 10941 (2015).
108. Anikeeva, P. O., Halpert, J. E. & Bawendi, M. G., & Bulovic´V. Electroluminescence from a mixed red-green-blue colloidal quantum dot monolayer. *Nano Lett.* **7**, 2196–2200 (2007).
109. Bae, W. K. et al. R/G/B/natural white light thin colloidal quantum dot-based light-emitting devices. *Adv. Mater.* **26**, 6387–6393 (2014).
110. Bae, W. K. et al. Multicolored light-emitting diodes based on all-quantum-dot multilayer films using layer-by-layer assembly method. *Nano Lett.* **10**, 2368–2373 (2010).
111. Kim, T.-H. et al. Heterogeneous stacking of nanodot monolayers by dry pick-and-place transfer and its applications in quantum dot light-emitting diodes. *Nat. Commun.* **4**, 2637 (2013).
112. Kagan, C. R., Murray, C. B. & Bawendi, M. G. Long range resonance transfer of electronic excitations in close packed CdSe quantum dot solids. *Phys. Rev. B* **54**, 8633–8643 (1996).
113. Kagan, C. R., Murray, C. B., Nirmal, M. & Bawendi, M. G. Electronic energy transfer in CdSe quantum dot solids. *Phys. Rev. Lett.* **76**, 1517 (1996).
114. Hsu, C. W. et al. Transparent displays enabled by resonant nanoparticle scattering. *Nat. Commun.* **5**, 3152 (2014).
115. Kim, H. Y. et al. Transparent InP quantum dot light-emitting diodes with ZrO2 electron transport layer and indium zinc oxide top electrode. *Adv. Funct. Mater.* **26**, 3454–3461 (2016).
116. Wood, V. et al. Air-stable operation of transparent, colloidal quantum dot based LEDs with a unipolar device architecture. *Nano Lett.* **10**, 24–29 (2010).
117. Kim, D.-Y., Han, Y. C., Kim, H. C., Jeong, E. G. & Choi, K. C. Highly transparent and flexible organic light-emitting diodes with structure optimized for anode/cathode multilayer electrodes. *Adv. Funct. Mater.* **25**, 7145–7153 (2015).
118. Kim, H.-M. et al. Semi-transparent quantum-dot light emitting diodes with an inverted structure. *J. Mater. Chem. C* **2**, 2259–2265 (2014).
119. Kim, Y. et al. Semitransparent quantum dot light-emitting diodes by cadmium-free colloidal quantum dots. *J. Nanosci. Nanotechnol.* **14**, 8636–8640 (2014).
120. Novoselov, K. S. et al. Electric field effect in atomically thin carbon films. *Science* **306**, 666–669 (2004).
121. Geim, A. K. & Novoselov, K. S. The rise of graphene. *Nat. Mater.* **6**, 183–191 (2007).
122. Choi, M. K. et al. Thermally controlled, patterned graphene transfer printing for transparent and wearable electronic/optoelectronic system. *Adv. Funct. Mater.* **25**, 7109–7118 (2015).
123. Lee, H. et al. An endoscope with integrated transparent bioelectronics and theranostic nanoparticles for colon cancer treatment. *Nat. Commun.* **6**, 10059 (2015).
124. Lee, H. et al. A graphene-based electrochemical device with thermoresponsive microneedles for diabetes monitoring and therapy. *Nat. Nanotechnol.* **11**, 566–572 (2016).
125. Kim, S. J. et al. Stretchable and transparent biointerface using cell-sheet-graphene hybrid for electrophysiology and therapy of skeletal muscle. *Adv. Funct. Mater.* **26**, 3207–3217 (2016).
126. Lee, J.-Y., Connor, S. T., Cui, Y. & Peumans, P. Solution-processed metal nanowire mesh transparent electrodes. *Nano Lett.* **8**, 689–692 (2008).
127. Yang, J. et al. Self-organized growth and self-assembly of nanostructures on 2D materials. *FlatChem* **5**, 50–68 (2017).
128. Seo, J.-T. et al. Fully transparent quantum dot light-emitting diode integrated with graphene anode and cathode. *ACS Nano* **8**, 12476–12482 (2014).
129. Hu, L., Kim, H. S., Lee, J.-Y., Peumans, P. & Cui, Y. Scalable coating and properties of transparent, flexible, silver nanowire electrodes. *ACS Nano* **4**, 2955–2963 (2010).
130. Kang, M.-G., Xu, T., Park, H. J., Luo, X. & Guo, L. J. Efficiency enhancement of organic solar cells using transparent plasmonic Ag nanowire electrodes. *Adv. Mater.* **22**, 4378–4383 (2010).
131. Yu, Z. et al. Highly flexible silver nanowire electrodes for shape-memory polymer light-emitting diodes. *Adv. Mater.* **23**, 664–668 (2011).
132. Hecht, D. S., Hu, L. & Irvin, G. Emerging transparent electrodes based on thin films of carbon nanotubes, graphene, and metallic nanostructures. *Adv. Mater.* **23**, 1482–1513 (2011).
133. Choi, S. et al. Stretchable heater using ligand-exchanged silver nanowire nanocomposite for wearable articular thermotherapy. *ACS Nano* **9**, 6626–6633 (2015).
134. Park, J. et al. Electromechanical cardioplasty using a wrapped elasto-conductive epicardial mesh. *Sci. Trans. Med.* **8**, 344ra96 (2016).
135. Jing, P. et al. Vacuum-free transparent quantum dot light-emitting diodes with silver nanowire cathode. *Sci. Rep.* **5**, 12499 (2015).
136. Wang, W., Peng, H. & Chen, S. Highly transparent quantum-dot light-emitting diodes with sputtered indium-tin-oxide electrodes. *J. Mater. Chem. C* **4**, 1838–1841 (2016).
137. Koo, J. H. et al. Wearable electrocardiogram monitor using carbon nanotube electronics and color-tunable organic light-emitting diodes. *ACS Nano* **11**, 10032–10041 (2017).
138. Kim, J., Lee, J., Son, D., Choi, M. K. & Kim, D.-H. Deformable devices with integrated functional nanomaterials for wearable electronics. *Nano Converg.* **3**, 4 (2016).
139. Jung, S. et al. Reverse-micelle-induced porous pressure-sensitive rubber for wearable human–machine interfaces. *Adv. Mater.* **26**, 4825–4830 (2014).
140. Lim, S. et al. Transparent and stretchable interactive human machine interface based on patterned graphene heterostructures. *Adv. Funct. Mater.* **25**, 375–383 (2015).
141. Choi, M. K. et al. Cephalopod-inspired miniaturized suction cups for smart medical skin. *Adv. Healthc. Mater.* **5**, 80–87 (2016).
142. Lee, H. et al. Wearable/disposable sweat-based glucose monitoring device with multistage transdermal drug delivery module. *Sci. Adv.* **3**, e1601314 (2017).
143. Jung, S., Lee, J., Hyeon, T., Lee, M. & Kim, D.-H. Fabric-based integrated energy devices for wearable activity monitors. *Adv. Mater.* **26**, 6329–6334 (2014).
144. Lee, Y., Kim, J., Koo, J. H., Kim, T.-H. & Kim, D.-H. Nanomaterials for bioelectronics and integrated medical systems. *Korean J. Chem. Eng.* **35**, 1–11 (2018).
145. Yu, K. J., Yan, Z., Han, M. & Rogers, J. A. Inorganic semiconducting materials for flexible and stretchable electronics. *npj Flex Electron* **1**, 4 (2017).
146. Choi, C. et al. Human-eye-inspired soft optoelectronic device using high-density MoS2-graphene curved image sensor array. *Nat. Commun.* **8**, 1664 (2017).
147. Choi, C., Choi, M. K., Hyeon, T. & Kim, D.-H. Nanomaterial-based soft electronics for healthcare applications. *ChemNanoMat* **2**, 1006–1017 (2016).
148. Kim, D. et al. Polyethylenimine ethoxylated-mediated all-solution-processed high-performance flexible inverted quantum dot-light-emitting device. *ACS Nano* **11**, 1982–1990 (2017).
149. Yang, X. et al. Highly flexible, electrically driven, top-emitting, quantum dot light-emitting stickers. *ACS Nano* **8**, 8224–8231 (2014).
150. Wang, C. et al. User-interactive electronic skin for instantaneous pressure visualization. *Nat. Mater.* **12**, 899–904 (2013).
151. Kim, J. et al. A wearable multiplexed silicon nonvolatile memory array using nanocrystal charge confinement. *Sci. Adv.* **2**, e1501101 (2016).
152. Lee, J. et al. Ultra-wideband multi-dye-sensitized upconverting nanoparticles for information security application. *Adv. Mater.* **29**, 1603169 (2017).
153. Lee, Y. et al. Wearable sensing systems with mechanically soft assemblies of nanoscale materials. *Adv. Mater. Technol.* **2**, 1700053 (2017).
154. Lee, W. et al. High-resolution spin-on-patterning of perovskite thin films for a multiplexed image sensor array. *Adv. Mater.* **29**, 1702902 (2017).
155. Son, D. et al. Colloidal synthesis of uniform-sized molybdenum disulfide nanosheets for wafer-scale flexible nonvolatile memory. *Adv. Mater.* **28**, 9326–9332 (2016).
156. Song, J.-K. et al. Wearable force touch sensor array using a flexible and transparent electrode. *Adv. Funct. Mater.* **27**, 1605286 (2017).
157. Lochner, C. M., Khan, Y., Pierre, A. & Arias, A. C. All-organic optoelectronic sensor for pulse oximetry. *Nat. Commun.* **5**, 5745 (2014).
158. Kim, T.-H. et al. Fully stretchable optoelectronic sensors based on colloidal quantum dots for sensing photoplethysmographic signals. *ACS Nano* **11**, 5992–6003 (2017).